Supplementary Information (SI) for Journal of Materials Chemistry C.

Supporting Information

808 nm Laser Excited Upconverting Hydrophilized Fluid Velocimetric Probe with a Record Sensitivity

Linke Zhang [a, +], Shijie Hu [a, +], Xubin Fu [a, *], Nianfeng Zhang [a], Feng Huang [a,d,e,*], Tao Pang [b], Hai Huang [c, *], An Xie [c], and Daqin Chen [a, d, e, *]

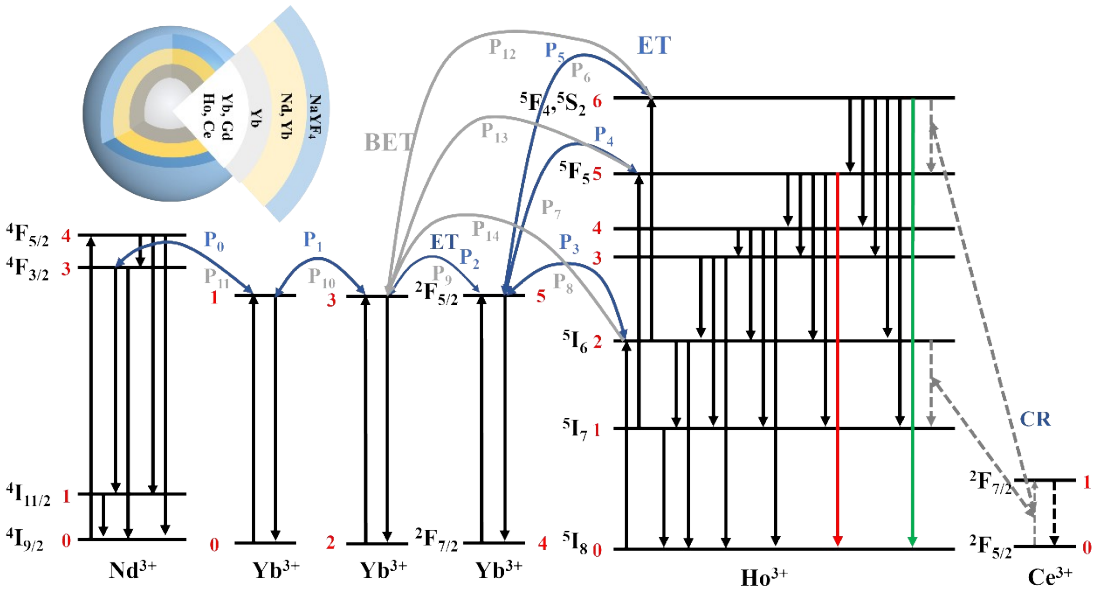

I. Numerical simulation

Scheme S1. Proposed energy transfer and migration channels in Yb-Ho-Ce co-doped upconversion system. Relevant simulation parameters were summarized in Table S1.

To numerically simulate the electronic transition processes, a two-photon upconversion energy transfer model has been devised. The luminescence intensity of the system is governed by a multitude of factors, including the laser pump power density, energy level absorption cross-sections, radiative transition probabilities, energy transfer rates, and cross-relaxation rates. For the sake of computational simplicity, non-radiative transition pathways, such as thermal relaxation and defect

scattering, are commonly disregarded. Consequently, the rate equations can be simplified to the following form:

$$\frac{dN_x}{dt} = w\sigma_{x-1}N_{x-1} - w\sigma_x N_x - A_{xy}N_x + P_{ij,kl}N_i N_l - S_{ij,kl}N_i N_l$$

The upconversion process of Yb-Ho-Ce co-doped upconversion system can be described by the energy transfer rate equation, based on the energy transfer upconversion process as shown in Fig. The rate equations for each energy level are derived as follows:

$$\frac{dN_{nd0}}{dt} = -\,w\sigma N_{nd0} + A_{nd1}N_{nd1} + A_{nd2}N_{nd2} + A_{nd3}N_{nd3}$$

$$\frac{dN_{nd1}}{dt} = -\,A_{nd1}N_{nd1} + A_{nd21}N_{nd2} + A_{nd31}N_{nd3} + p_0N_{nd2}N_{yb0} - p_{11}N_{yb1}N_{nd1}$$

$$\frac{dN_{nd2}}{dt} = -\,A_{nd2}N_{nd2} - A_{nd21}N_{nd2} + A_{nd32}N_{nd3} - p_0N_{nd2}N_{yb0} + p_{11}N_{yb1}N_{nd1}$$

$$\frac{dN_{nd3}}{dt} = w\sigma N_{nd0} - A_{nd3}N_{nd3} - A_{nd31}N_{nd3} - A_{nd32}N_{nd3}$$

$$\frac{dN_{yb0}}{dt} = -\,p_0N_{nd2}N_{yb0} + p_1N_{yb1}N_{yb2} - p_{10}N_{yb3}N_{yb0} + p_{11}N_{yb1}N_{nd1} + A_{yb10}N_{yb1}$$

$$\frac{dN_{yb1}}{dt} = p_0N_{nd2}N_{yb0} - p_1N_{yb1}N_{yb2} + p_{10}N_{yb3}N_{yb0} - p_{11}N_{yb1}N_{nd1} - A_{yb10}N_{yb1}$$

$$\frac{dN_{yb2}}{dt} = -\,p_1N_{yb1}N_{yb2} + p_2N_{yb3}N_{yb4} - p_9N_{yb5}N_{yb2} + p_{10}N_{yb3}N_{yb0} + A_{yb32}N_{yb3} - p_{12}N_6N_{yb2} - p_{13}N_5N_{yb2} - p_{14}N_2N_{yb2}$$

$$\frac{dN_{yb3}}{dt} = p_1N_{yb1}N_{yb2} - p_2N_{yb3}N_{yb4} + p_9N_{yb5}N_{yb2} - p_{10}N_{yb3}N_{yb0} - A_{yb32}N_{yb3} + p_{12}N_6N_{yb2} + p_{13}N_5N_{yb2} + p_{14}N_2N_{yb2}$$

$$\frac{dN_{yb4}}{dt} = - p_2N_{yb3}N_{yb4} + p_3N_{yb5}N_0 + p_4N_{yb5}N_1 + p_5N_{yb5}N_2 - p_6N_6N_{yb4} - p_7N_5N_{yb4} - p_8N_2N_{yb4} + p_9N_{yb5}N_{yb2} + A_{yb54}N_{yb5}$$

$$\frac{dN_{yb5}}{dt} = p_2N_{yb3}N_{yb4} - p_3N_{yb5}N_0 - p_4N_{yb5}N_1 - p_5N_{yb5}N_2 + p_6N_6N_{yb4} + p_7N_5N_{yb4} + p_8N_2N_{yb4} - p_9N_{yb5}N_{yb2} - A_{yb54}N_{yb5}$$

$$\frac{dN_{Ho0}}{dt} = - p_3N_{yb5}N_0 + p_8N_2N_{yb4} + A_{10}N_1 + A_{20}N_2 + A_{30}N_3 + A_{40}N_4 + A_{50}N_5 + A_{60}N_6 + p_{14}N_2N_{yb2}$$

$$\frac{dN_{Ho1}}{dt} = S_1N_{ce0}N_2 - p_4N_{yb5}N_1 + p_7N_5N_{yb4} - A_{10}N_1 + A_{21}N_2 + A_{31}N_3 + A_{41}N_4 + A_{51}N_5 + A_{61}N_6 + p_{13}N_5N_{yb2}$$

$$\frac{dN_{Ho2}}{dt} = - S_1N_{ce0}N_2 - p_5N_{yb5}N_2 + p_3N_{yb5}N_0 + p_6N_6N_{yb4} - p_8N_2N_{yb4} - A_{20}N_2 - A_{21}N_2 + A_{32}N_3 + A_{42}N_4 + A_{52}N_5 + A_{62}N_6 + p_{12}N_6N_{yb2} - p_{14}N_2N_{yb2}$$

$$\frac{dN_{Ho3}}{dt} = - A_{30}N_3 - A_{31}N_3 - A_{32}N_3 + A_{43}N_4 + A_{53}N_5 + A_{63}N_6$$

$$\frac{dN_{Ho4}}{dt} = - A_{40}N_4 - A_{41}N_4 - A_{42}N_4 - A_{43}N_4 + A_{54}N_5 + A_{64}N_6$$

$$\frac{dN_{Ho5}}{dt} = S_2N_{ce0}N_6 + p_4N_{yb5}N_1 - p_7N_5N_{yb4} - A_{50}N_5 - A_{51}N_5 - A_{52}N_5 - A_{53}N_5 - A_{54}N_5 + A_{65}N_6 - p_{13}N_5N_{yb2}$$

$$\frac{dN_{Ho6}}{dt} = - S_2N_{ce0}N_6 + p_5N_{yb5}N_2 - p_6N_6N_{yb4} - A_{60}N_6 - A_{61}N_6 - A_{62}N_6 - A_{63}N_6 - A_{64}N_6 - A_{65}N_6 - p_{12}N_6N_{yb2}$$

$$\frac{dN_{ce0}}{dt} = - S_1N_{ce0}N_2 - S_2N_{ce0}N_6 + A_{ce10}N_{ce1}$$

$$\frac{dN_{ce1}}{dt} = S_1N_{ce0}N_2 + S_2N_{ce0}N_6 - A_{ce10}N_{ce1}$$

where N_x represents the population of the corresponding energy level, w is the power density of the laser, σ_x is the absorption cross-section of the corresponding energy level, A_{xy} (refer to Zheng et al.)[S1] is the rate of radiative transition from energy level x to energy level y, $P_{ij,kl}$ is the rate of energy transfer occurring through the donor i → j transition and the acceptor k → l transition, and $S_{ij,kl}$ is the rate of cross-relaxation occurring through the donor i → j transition and the acceptor k → l transition. Rate equation-based theoretical analyses and simulations were conducted using python to obtain the non-steady-state population density evolution of the green-emitting and red-emitting states (N_{Ho6}, N_{Ho5}) of Ho^{3+}.

Table S1. The parameters used in the numerical simulation for the Yb-Ho-Ce co-doped upconversion system.

Cross-relaxation rate ($cm^3\ s^{-1}$)	
S_1	S_2
3×10^{-17}	5×10^{-17}

Energy transfer rate ($cm^3\ s^{-1}$)				
P_0	P_1	P_2	P_3	P_4
9×10^{-17}	1×10^{-18}	1×10^{-18}	6×10^{-18}	1.5×10^{-18}
P_5	P_6	P_7	P_8	P_9
3×10^{-18}	9×10^{-18}	1×10^{-19}	1×10^{-19}	6×10^{-20}
P_{10}	P_{11}	P_{12}	P_{13}	P_{14}
1×10^{-20}	3×10^{-20}	6×10^{-21}	1×10^{-21}	3×10^{-21}

Initial population density (cm^{-3})				
N_{nd0}	N_{yb0}	N_{yb2}	N_0	N_{ce0}
8.28×10^{21}	2.76×10^{21}	2.76×10^{21}	2.76×10^{20}	1.38×10^{21}

$w = 2\times10^{22}\ cm^{-2}\ s^{-1}$ $\sigma = 2.5\times10^{-19}\ cm^2$

Reference

[S1] K. Huang, H. Qiu, X. Zhang, W. Luo, Y. Chen, J. Zhang, Y. Chen, G. Wang, K. Zheng, *Angewandte Chemie*, 2023, **135**, e202218491.

Table S2. Calibration of flow velocity and measurement error by fitting curves.

	Set velocity (cm/s)	FIR	Measured velocity (cm/s)	Error
①	3.396	1.886	3.719	8.69%
②	5.756	1.827	5.889	2.26%
③	8.116	1.779	8.519	4.73%
④	11.066	1.750	11.660	5.09%

II. Supplementary Figures

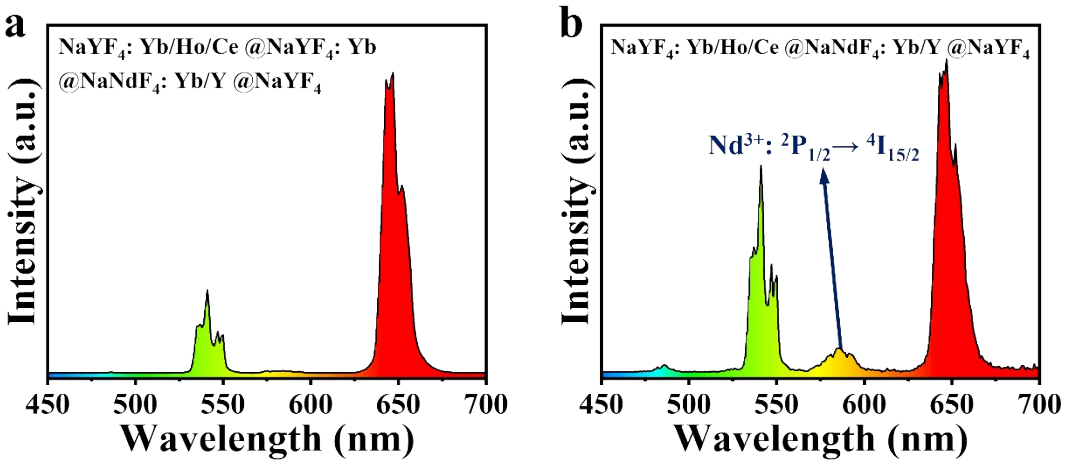

Figure S1. Upconversion emission spectra of the nanostructures, **(a)** with and **(b)** without the Yb^{3+}-content transition layer under 808 nm CW laser excitation.

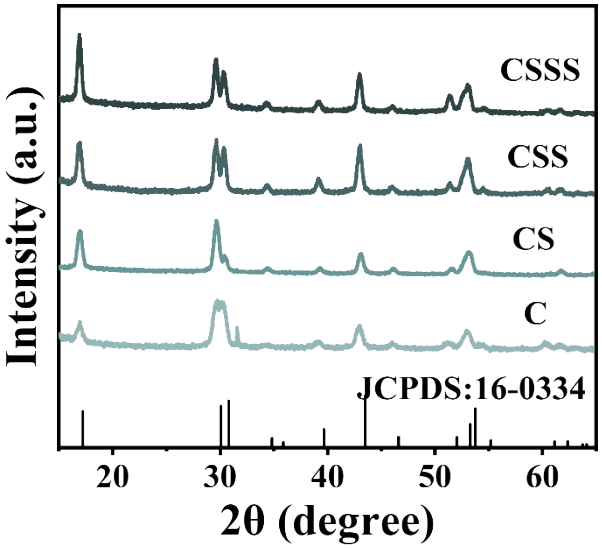

Figure S2. The XRD patterns of the C, CS, CSS and CSSS products.

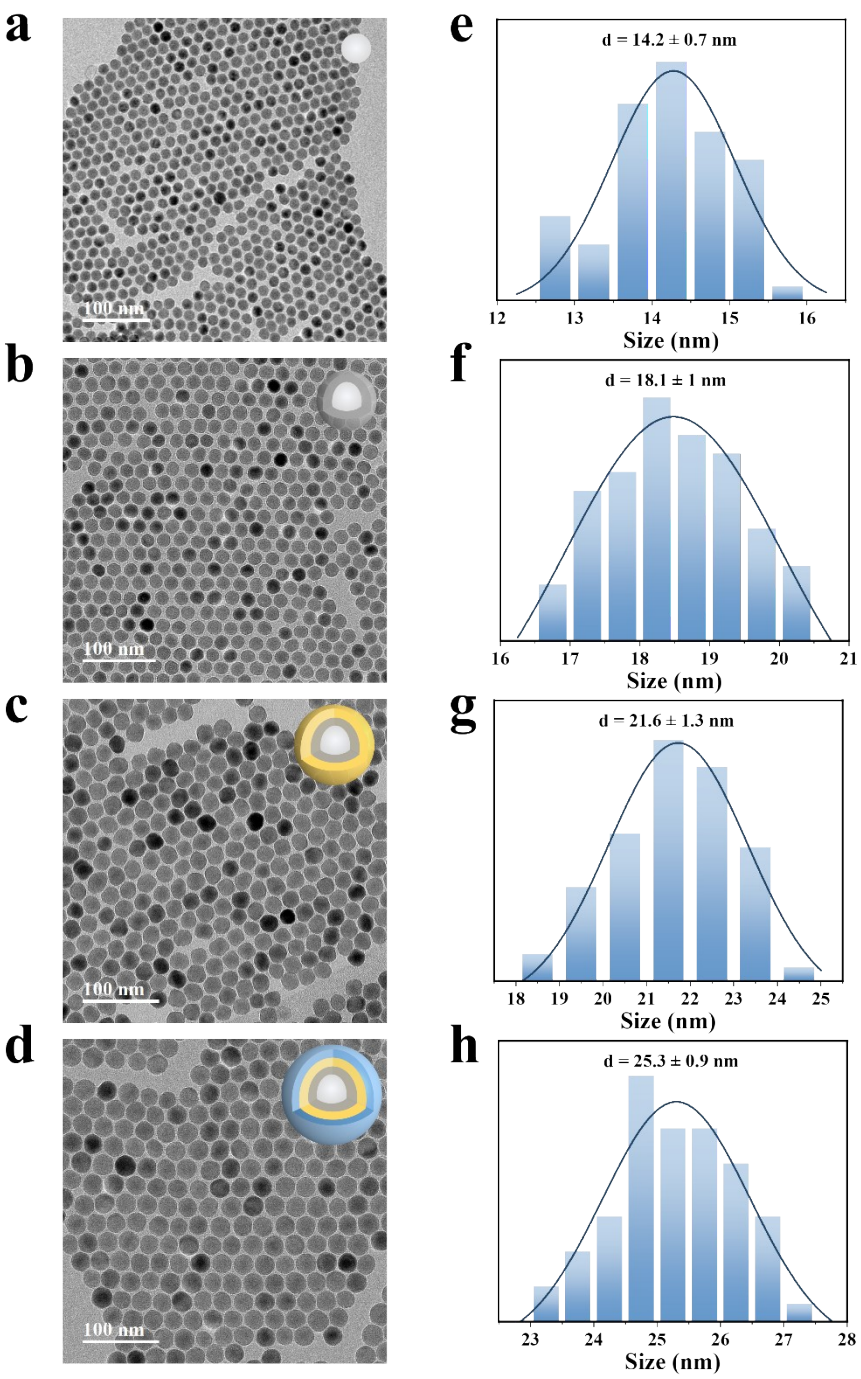

Figure S3. (a-d) The TEM images and **(e-h)** corresponding size distributions of the C, CS, CSS and CSSS products.

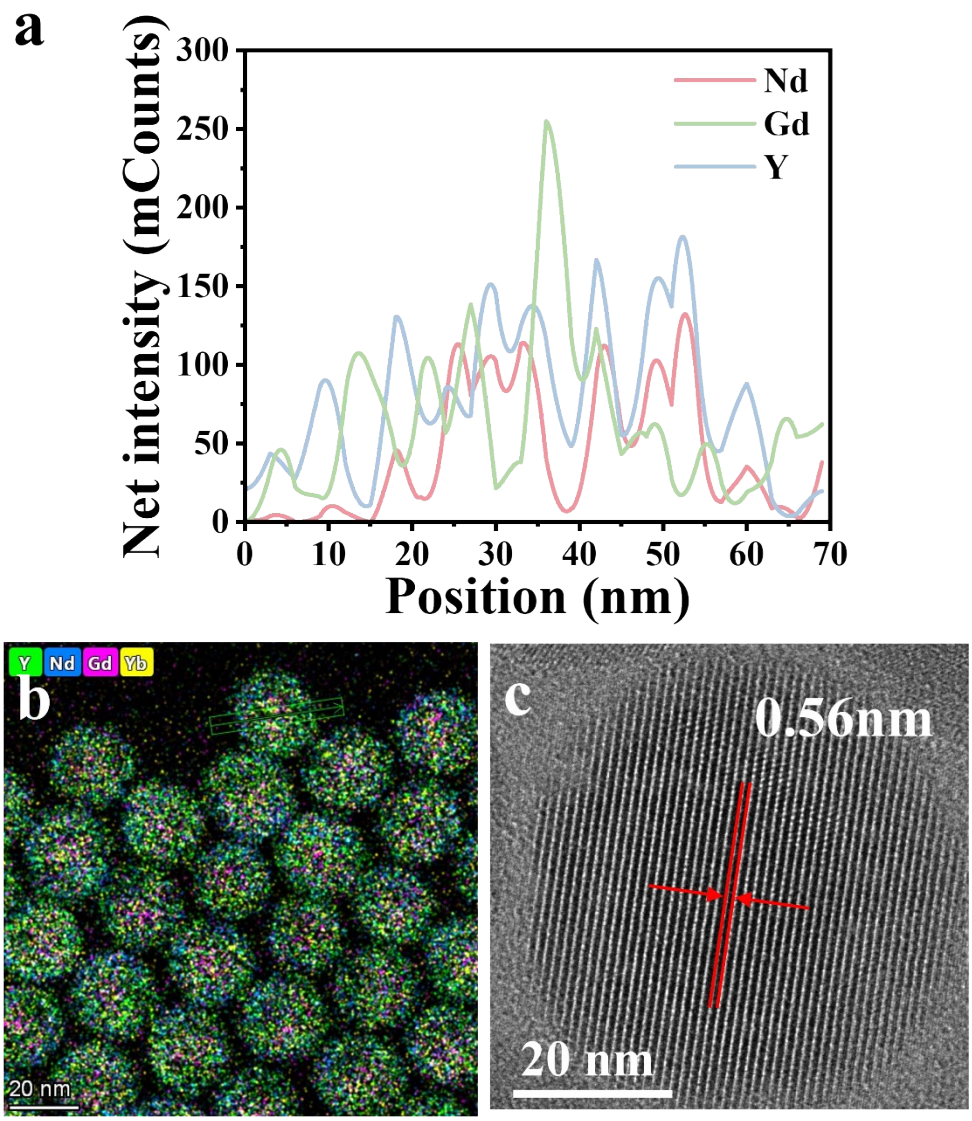

Figure S4. **(a)** Elemental line scan (obtained along the dashed line in **b**) of a representative CSSS nanoparticles, showing the spatial distribution of the Y, Nd, Gd and Yb elements. **(b)** Elemental mapping image of the CSSS products. **(c)** HRTEM image of the CSSS products.

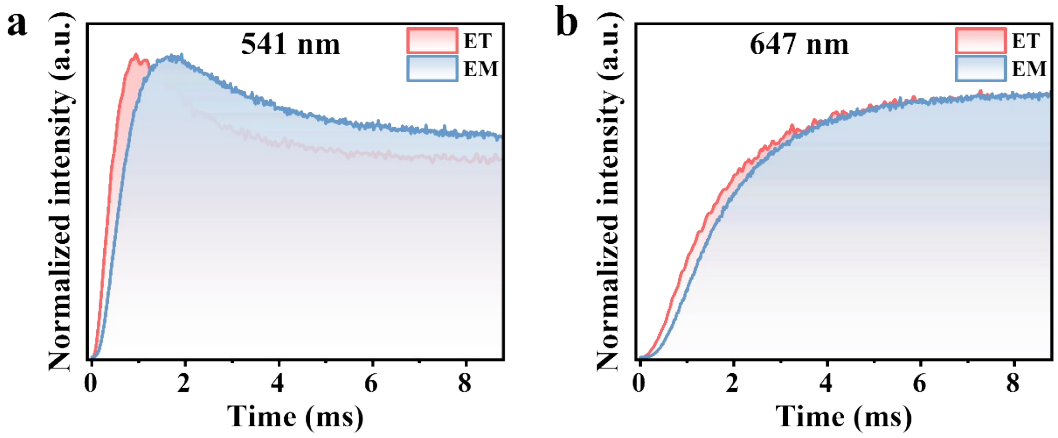

Figure S5. The time-dependent intensity profiles of Ho^{3+} emissions at **(a)** 541 nm and **(b)** 647 nm for the energy migration and energy transfer processes. These EM and ET curves were obtained for particles with and without the two additional shells.

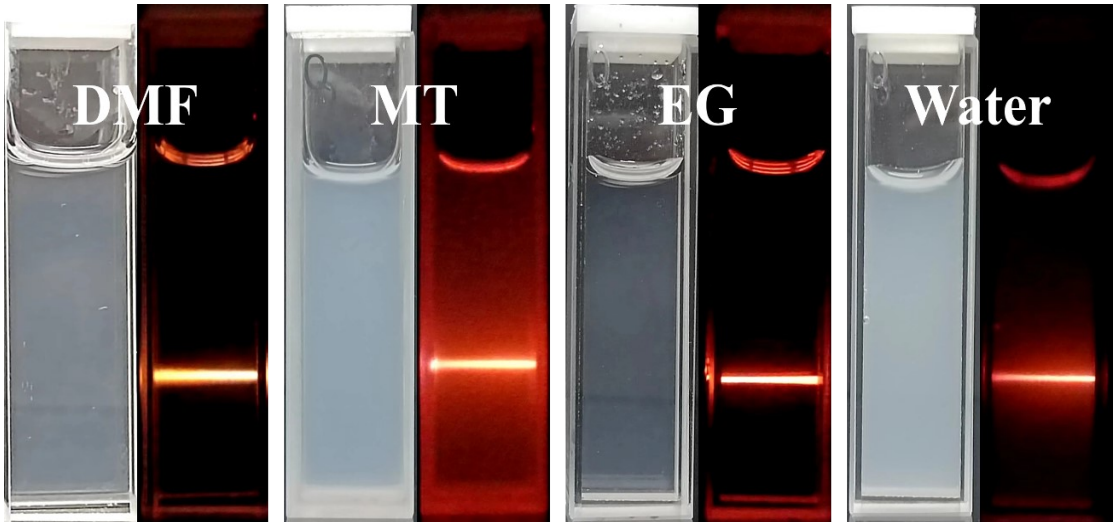

Figure S6. The photos of CSSS nanoparticles dispersed in various polar solvents (e.g. dimethylformamide, methanol, ethylene glycol and water) under lighting, or upon the 808 nm laser excitation in darkroom.

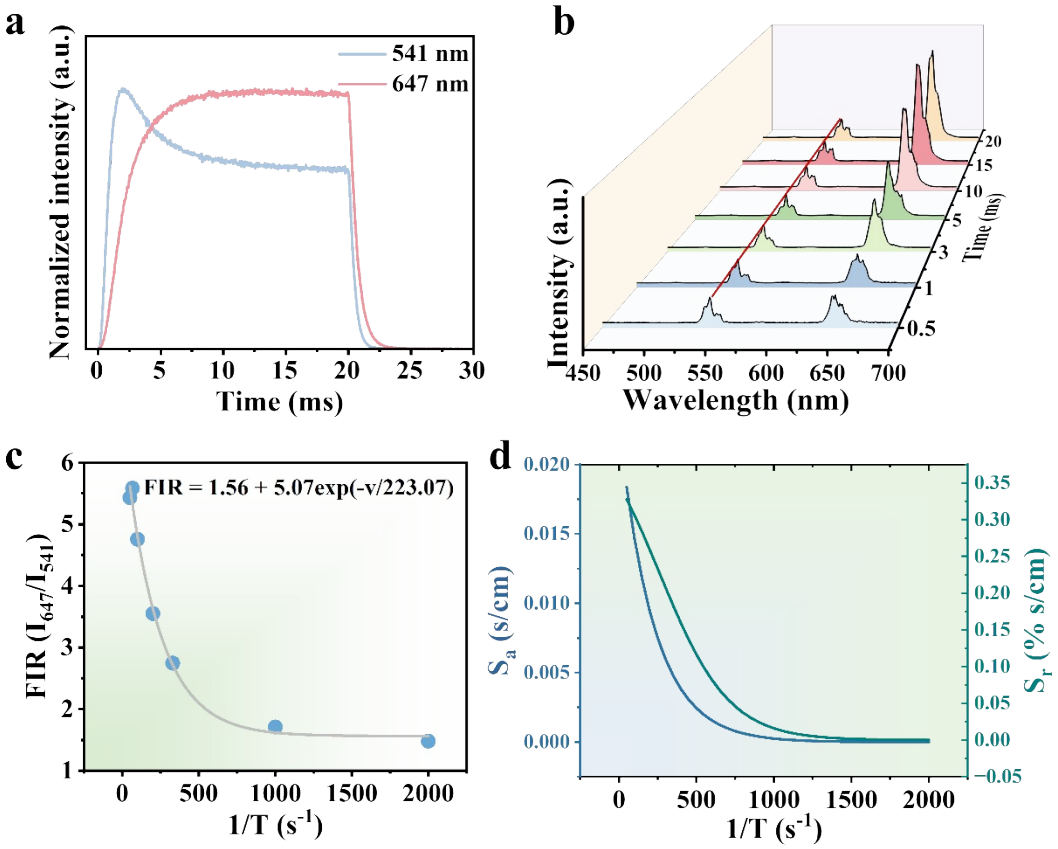

Figure S7. Hydrophilic CSSS nanoparticles**. (a)** Time-dependent intensity profiles of Ho^{3+} emission at 541 nm and 647 nm, under the excitation of 808 nm pulsed laser (pulse width of 20 ms). **(b)** UC emission spectra under 808 nm pulsed laser excitation (Pulse width from 0.5 m to 20 ms). **(c)** Plots of FIR (I_{647}/I_{541}) versus pulse duration, accompanied by e-exponential fitting lines. **(d)** Calculated values of S_a and S_r for these nanoparticles.

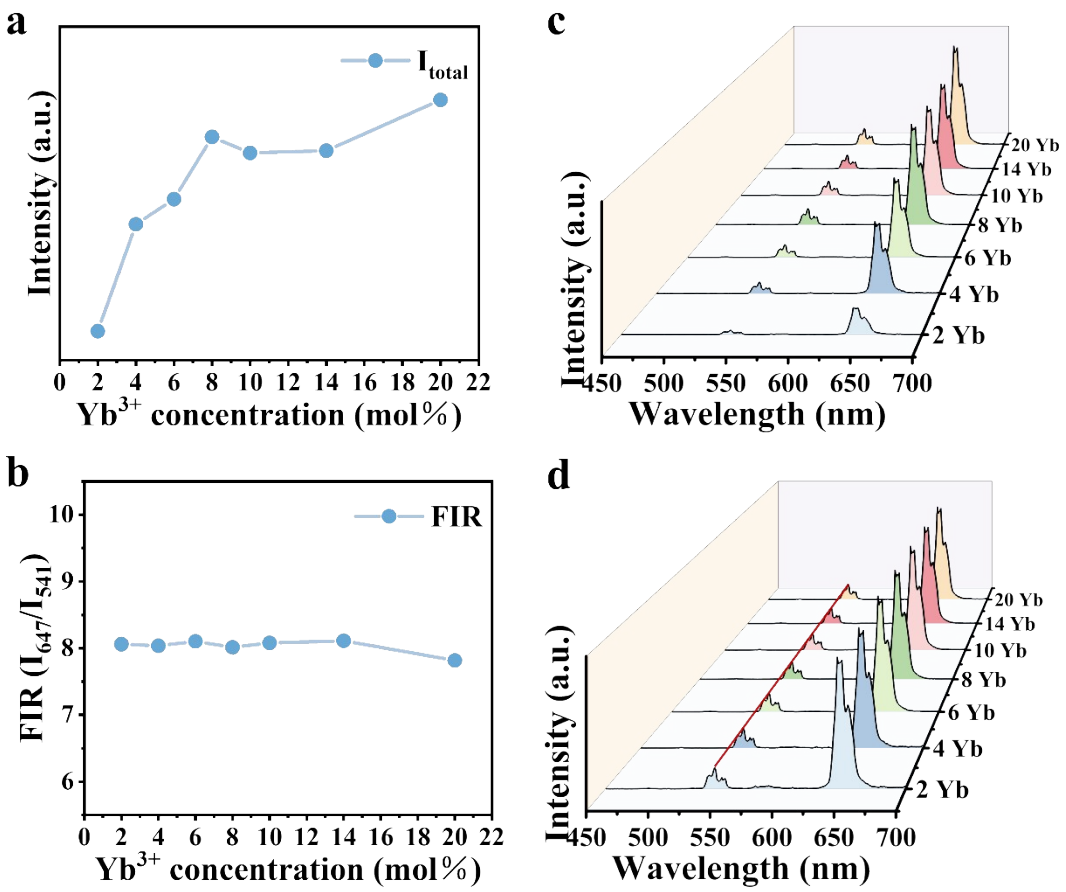

Figure S8. (a) Integral UC luminescent intensity of various CSSS-x-y (x=2, 4, 6, 8, 10, 14, 20, y=20) samples. **(b)** Corresponding FIR (I_{647}/I_{541}) variations. **(c)** UC emission spectra of CSSS-x-y (x=2, 4, 6, 8, 10, 14, 20, y=20) nanoparticles under 808 nm CW laser excitation. **(d)** UC emission spectra (normalized at 541 nm) of CSSS-x-y (x=2, 4, 6, 8, 10, 14, 20, y=20) nanoparticles under 808 nm CW laser excitation.

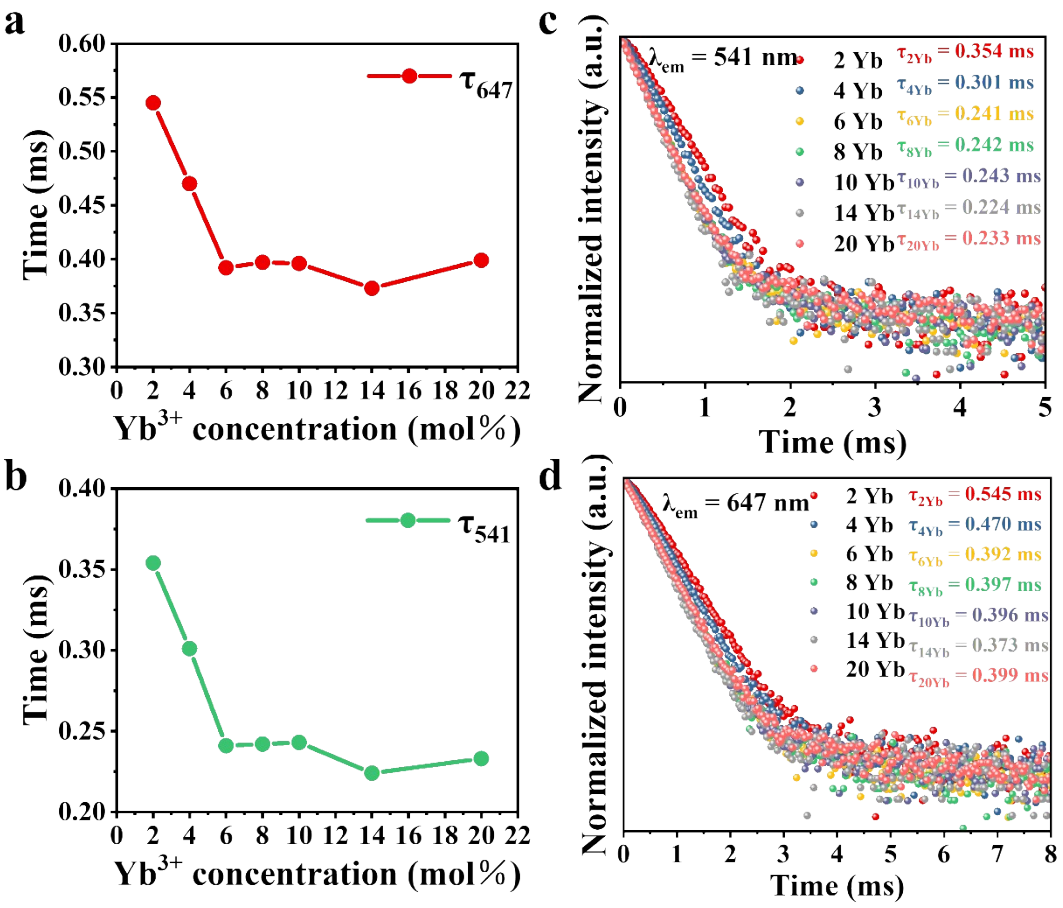

Figure S9. (a-b) The luminescent lifetimes of Ho^{3+} emissions at 647 nm and 541 nm, for various CSSS-x-y (x=2, 4, 6, 8, 10, 14, 20, y=20) samples. **(c)** UC luminescence decay curves of Ho^{3+} emission at 541 nm under 808 nm pulsed laser excitation (20 ms) in CSSS-x-y (x=2, 4, 6, 8, 10, 14, 20, y=20) nanoparticles. **(d)** UC luminescence decay curves of Ho^{3+} emission at 647 nm under 808 nm pulsed laser excitation (20 ms) in CSSS-x-y (x=2, 4, 6, 8, 10, 14, 20, y=20) nanoparticles.

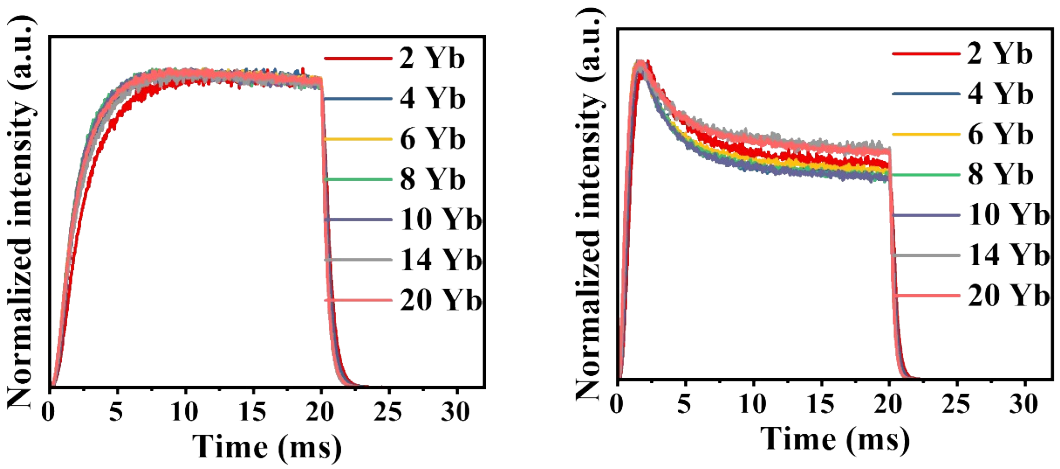

Figure S10. Time-dependent intensity profiles of **(a)** 647 nm and **(b)** 541 nm emissions of CSSS-x-y (x=2, 4, 6, 8, 10, 14, 20, y=20) samples.

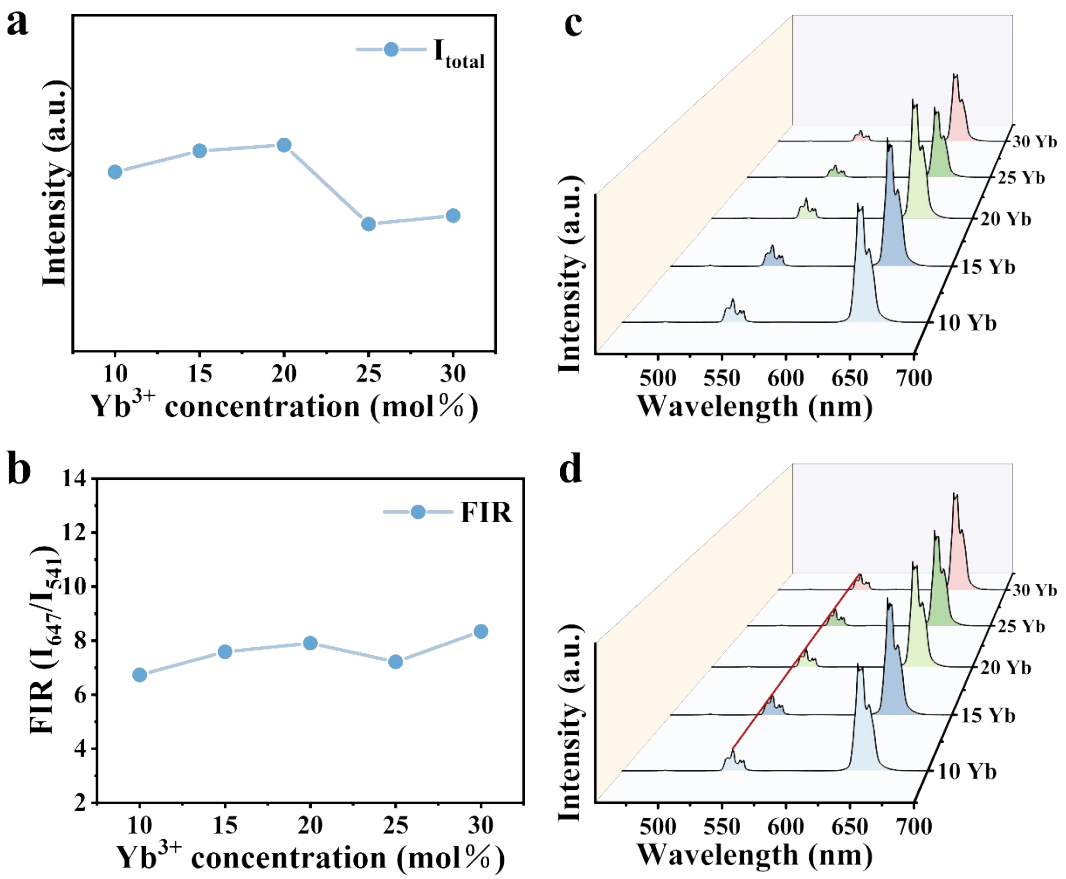

Figure S11. (a) Integral UC luminescent intensity of various CSSS-x-y (x=10, y=10, 15, 20, 25, 30) samples. **(b)** Corresponding FIR (I_{647}/I_{541}) variations. **(c)** UC emission spectra of CSSS-x-y (x=10, y=10, 15, 20, 25, 30) nanoparticles under 808 nm CW laser excitation. **(d)** UC emission spectra (normalized at 541 nm) of CSSS-x-y (x=10, y=10, 15, 20, 25, 30) nanoparticles under 808 nm CW laser excitation.

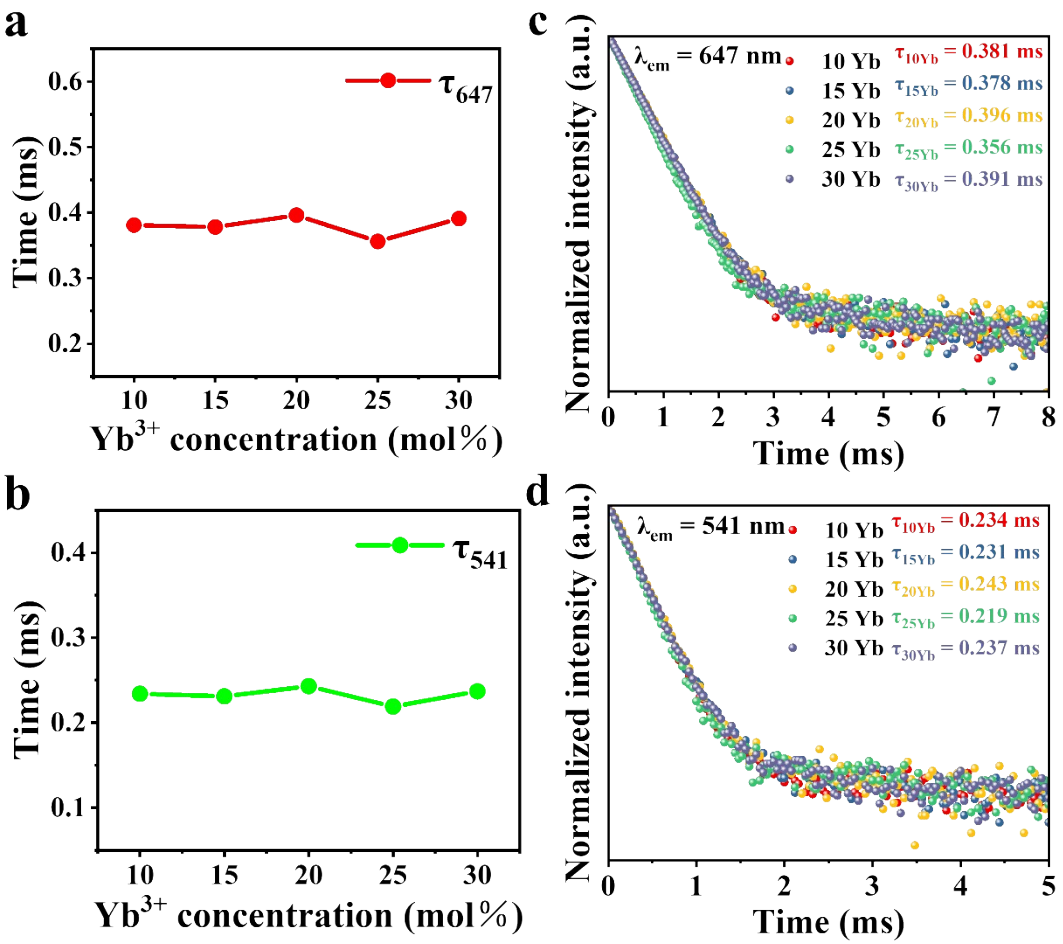

Figure 12. (a-b) The luminescent lifetimes of Ho^{3+} emissions at 647 nm and 541 nm, for various CSSS-x-y (x=10, y=10, 15, 20, 25, 30) samples. **(c)** UC luminescence decay curves of Ho^{3+} emission at 541 nm under 808 nm pulsed laser excitation (20 ms) in CSSS-x-y (x=10, y=10, 15, 20, 25, 30) nanoparticles. **(d)** UC luminescence decay curves of Ho^{3+} emission at 647 nm under 808 nm pulsed laser excitation (20 ms) in CSSS-x-y (x=10, y=10, 15, 20, 25, 30) nanoparticles.

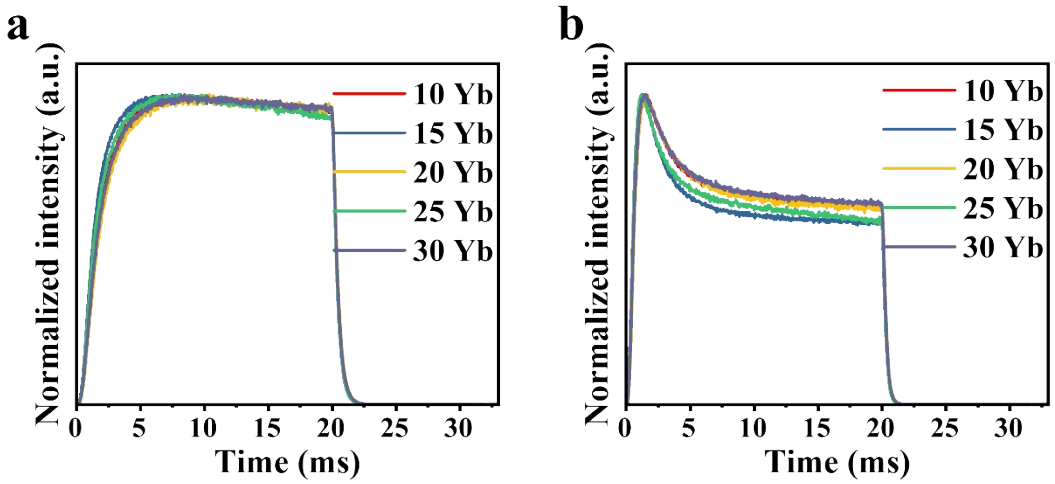

Figure S13. Time-dependent intensity profiles of **(a)** 647 nm and **(b)** 541 nm emissions of CSSS-x-y (x=10, y=10, 15, 20, 25, 30) samples.

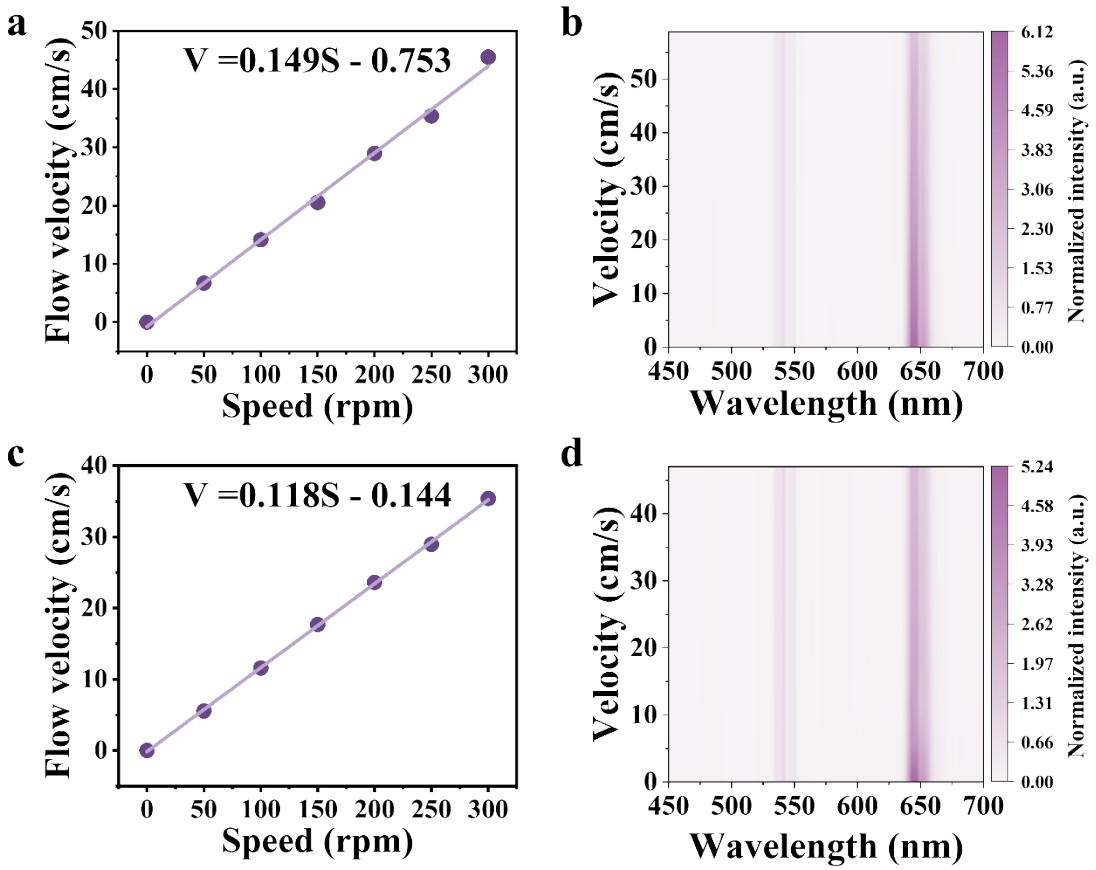

Figure S14. (a) The correspondence between the flow velocity of samples dispersed in cyclohexane and the rotational speed of the peristaltic pump. **(b)** UC emission spectra of CSSS-x-y (x=10, y=20) samples at different velocities. **(c)** The correspondence between the flow velocity of samples dispersed in water and the rotational speed of the peristaltic pump. **(d)** UC emission spectra of CSSS-x-y (x=10, y=20) water-soluble samples at different velocities.

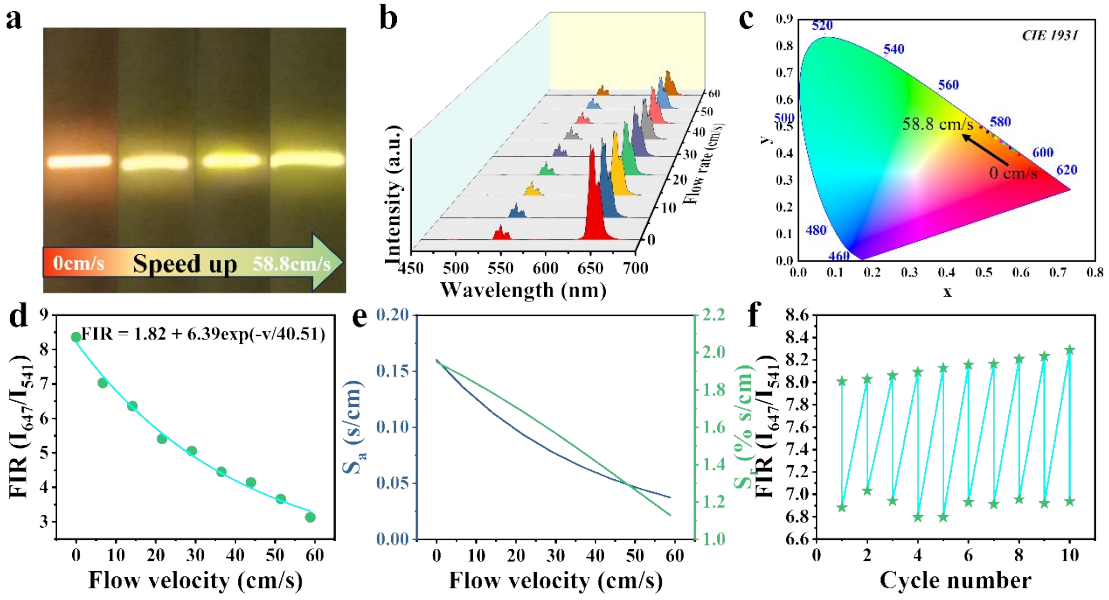

Figure S15. (a) Photos of the fluid in the tube with various flow velocities under 808 nm laser excitation. Dispersed in the fluid are the CSSS-x-y (x=10, y=20) nanoparticles. **(b)** UC emission spectra measured at different flowing velocity. **(c)** Corresponding emission colors indexed on the chromaticity diagram (CIE 1931). **(d)** The plots of FIR (I_{647}/I_{541}) versus flow velocity, accompanied by e-exponential fitting lines. **(e)** Calculated values of Sa and Sr for those samples. **(f)** The FIR during 10 cycles of acceleration and deceleration between speeds of 0 cm/s and 14.15 cm/s.

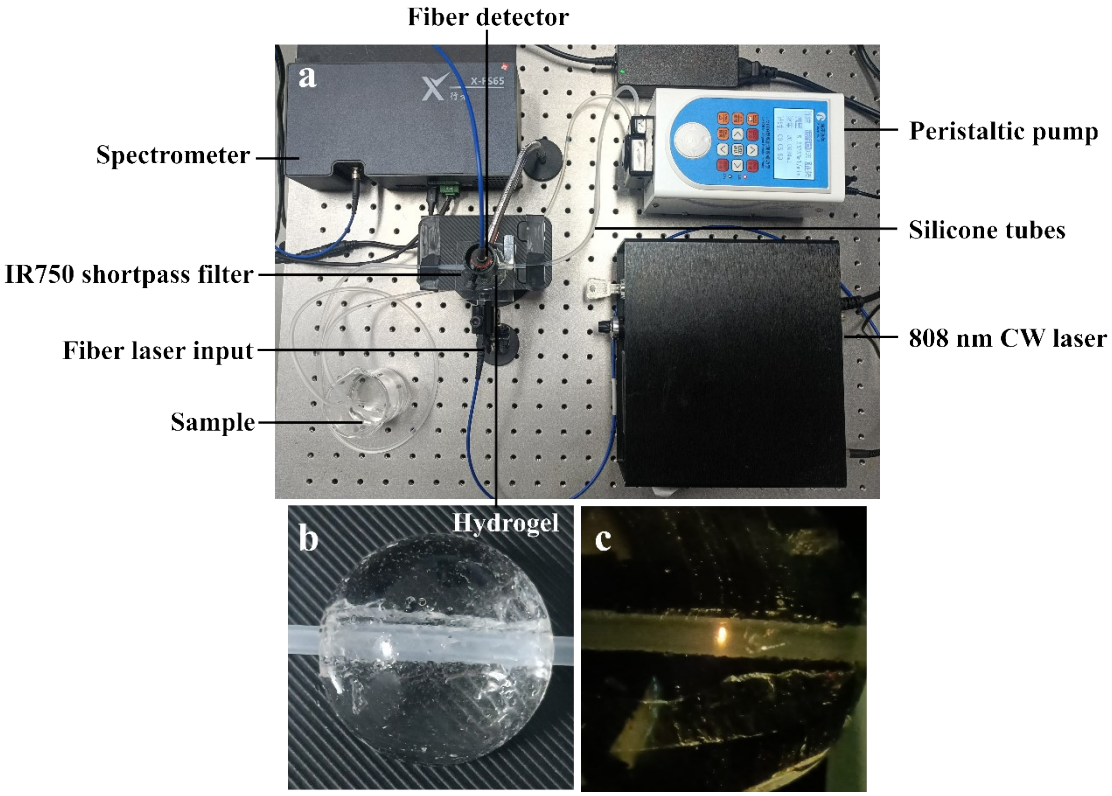

Figure S16. (a) The photos of experimental apparatus for a fluid velocimetry application demonstration. **(b)** The photos of hydrogel (sodium alginate) over silicone tube. **(c)** is **(b)** upon the 808 nm laser excitation in darkroom.